
Proceedings Paper:
Li, X, Mao, X orcid.org/0000-0002-9004-2081 and Jaworski, AJ (2017) Hydrodynamic characterization of gas-solids fluidized beds by means of electrical capacitance tomography. In: Proceedings of ASEE17. International conference on advances in energy systems and environmental engineering (ASEE17), 02-05 Jul 2017, Wroclaw, Poland. .

Hydrodynamic characterization of gas-solids fluidized beds by means of electrical capacitance tomography

Xiaoxu LI[1], Xiaoan MAO[1], and Artur J. JAWORSKI[1,*]

[1]Faculty of Engineering, University of Leeds, Woodhouse Lane, LS2 9JT, Leeds, UK

Abstract. Fluidized beds have been widely utilized in many industrial applications especially in energy conversion sectors, such as power generation and steam generation. One of the popular uses is to utilize fluidized bed combustion processes in urban waste management in order to produce additional district heating capabilities. However, the understanding of the internal fluid flow structure of the gas-solids fluidized beds is still inadequate due to its complex and chaotic nature. Electrical capacitance tomography (ECT) has been developed as a non-invasive and non-intrusive measurement technique and applied in the area of researching the flow physics of gas-solids fluidized beds. In this paper, a customized ECT twin-plane sensor (with 10 mm long measuring electrodes) has been designed and constructed to further study the fluid flow structure and processes within a bench-scale gas-solids fluidized bed. Conventional cross-correlation techniques were applied to derive the averaged axial bubble rising velocity. In addition, conventional cross-correlation techniques on a pixel-by-pixel basis were utilized to extract axial bubble rising velocity. The results were presented in three dimensional representations and were compared with empirical correlations as well as the above mentioned conventional methods. The temporal and spatial evolution of the bed behaviour observed from the three dimensional velocity profiles is analysed.

1 Introduction

Gas-solids fluidized beds have been broadly utilized in industrial applications owing to their various advantages, such as the liquid-like behaviour of solids particles, rapid mixing and high mass and heat transfer rate [1]. The main application areas are within energy conversion sectors, such as power generation and steam generation [2]. One of the popular uses is to utilize fluidized bed combustion processes in urban waste management in order to produce additional district heating capabilities [3]. However, the understanding of the internal fluid flow structure (especially bubbling regime) of the gas-solids fluidized beds is still inadequate due to its complex and chaotic nature. This unavoidably possesses challenges to the measurement techniques which are employed and are expected to produce reliable and accurate data for safe and optimal industrial operation [4].

* Corresponding author: a.j.jaworski@leeds.ac.uk

Numerous traditional measurement techniques have been tried out by previous researchers. For example, capacitance probes [5] were applied to derive bubble size (pierced length) and bubble frequency while cross correlation techniques were utilized to detect the rise velocity of a single bubble with two separated probes [6]. Fibre optic probes were employed to not only determine local solid particles' movements and the particle concentration [7] but also to characterize bubble features such as bubble size, bubble frequency, bubble rising velocity and bubble size distribution. Pressure transducers which are inserted into the bed body were implemented to determine the expanded bed height and bubble travelling time which was ultimately used to extract the bubble rising velocity [8]. However, all the aforementioned measurement techniques are not only of point-wise nature which means they are not able to effectively map the whole cross sectional area but also of intrusive nature, which inevitably introduces disturbance and interference with the internal fluid flow within the gas-solids fluidized beds [9].

Electrical capacitance tomography (ECT) has been developed for decades as a non-invasive and non-intrusive measurement technique, which can provide qualitative and quantitative data in monitoring a multi-phase fluid flow system by measuring the electrical capacitances between sets of electrodes placed around a process vessel [10]. ECT has the advantage of being simple to construct, fast in measurement speed, of low cost and able to withstand harsh operating conditions, i.e. high temperatures and pressures.

Recently, a considerable amount of literature has been published around the theme of bubble behaviour in fluidized beds as the characteristics of the bubbles, to a large extent, influence or determine the gas-solids mixing intensity and the mass and heat transfer rates. For example, bubble size has been investigated by Halow et al. [11] though debates still exist on how the bubble boundary was chosen. Another important parameter in characterizing bubble behaviour is bubble rising velocity. In practice, the bubble rising velocity can be derived by applying the cross-correlation techniques with a twin-plane ECT sensor whose two measuring planes are separated by a certain distance. Although several researchers have obtained results of the bubble rising velocity, few of them had evaluated the results with empirical correlations and also the system error caused by applying certain sampling rates using the cross-correlation techniques. Moreover, previous utilization of the cross-correlation techniques was mostly focused on the cross-sectional bubble rising velocity. Very few studies have been conducted yet to investigate the three dimensional representation on pixel-by-pixel basis.

This paper is aimed at investigating the bubble rising velocity by means of ECT measurement techniques. The main objectives are: (1) to derive the bubble rising velocity and compare and evaluate the results with widely used empirical correlations by means of conventional cross-correlation techniques, and (2) to investigate and evaluate the pixel-by-pixel approach in revealing the three dimensional representation of the bubble rising velocity. The temporal and spatial evolution of the bed behaviour observed from the three dimensional velocity profiles will be analysed.

2 Experimental

A customized experimental rig was designed and fabricated to investigate the bubble properties and a schematic drawing of the set-up is presented in Fig. 1. The fluidizing medium was ambient air and was provided by a compressed air cylinder. A needle valve acts as the isolation valve and controls the air flowing into the fluidized bed. The gas flow rate was measured by a float type flow meter before the air was introduced into the bed. The corresponding gas superficial velocity was converted from the gas flow rate by being divided by the cross-sectional area. The bench-scale gas-solids fluidized bed is composed of a 59 mm internal diameter (3 mm wall thickness) acrylic pipe with the length of 1 meter which was

designed to prevent any perturbation that may occur on the inside of the fluidized bed and also to allow visual observation to assist preliminary qualitative analysis. A perforated PVC distributor was designed and sandwiched by flanges between the bed pipe and the air plenum which was designed to direct and even out the upward air flow. The distributor has 48 holes of 1 mm diameter giving the total area of the holes in the distributor of 3.768 x 10-5 m2 (1.38% of the total effective area). A piece of fine mesh was placed on the air distributor to prevent any particles from leaking downwards. Silica sand was used as granular material. The density of the silica sand is 2650 kg/m^3, and its mean diameter is 276 microns, and so it belongs to the Geldard Group B particles for fluidization [12]. In order to prevent the solids from blowing out of the bed, a customized cap in which a piece of fine mesh is embedded was designed, constructed and mounted on top of the bed pipe. The static height of the fluidized bed is kept at 170 mm.

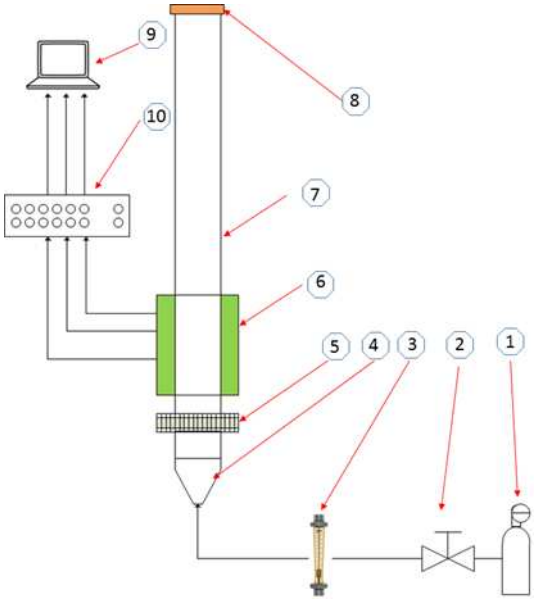

Fig. 1. Schematic drawing for experimental set-up: 1. Compressed air cylinder; 2. Needle valve; 3.Float flowmeter; 4.Plenum; 5.Air distributor; 6.Twin-plane ECT sensor; 7.Fluidized bed vessel; 8.Top-end cap; 9.Host PC; 10.Capacitance measurement unit.

The ECT measurement system used in the present study is the PTL300E system manufactured by Process Tomography, Ltd., Cheshire, UK. The system is a computer-controlled twin-plane ECT measurement system with the capability of recording and observing inter-electrode capacitance values and reconstructed image data at either one or two measurement planes. The flow detection is accomplished by a customized twin-plane ECT sensor whose layout is shown in Fig.2. There are two sets of measuring electrodes (with length of 10 mm) and three sets of guard electrodes which were designed to keep the electrostatic field inside the sensor as two-dimensional as possible for configuration calibration. Two axial earthed screens were placed at both ends of the sensor to prevent external noise signals or variations in the stray capacitance to earth which would otherwise predominate and corrupt the measurements. The tasks of image reconstruction and display are mainly executed by the PTL ECT32v2 software. This is a comprehensive suite of programs enabling the PTL300E system to be configured, calibrated, and utilized to record inter-electrode capacitance data files and to reconstruct them into image files at user-defined

speeds. The maximum image capturing speed in all the experiments conducted was kept at 200 frames per second (fps). It can also permit the PTL300E system to display and playback the captured capacitance and permittivity image data.

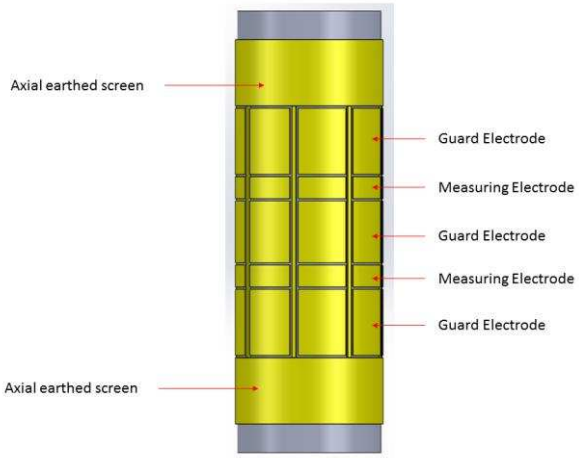

Fig. 2. Layout of the twin-plane ECT sensor.

The summarized experimental conditions relating to both the bench-scale gas-solids fluidized bed and the ECT measurement system are present in Table 1. Besides, the minimum fluidization velocity and the minimum slugging velocity have been determined as 5.54 cm/s and 8.89 cm/s, respectively according to previous research work [13]. These will be used as references to define the boundaries of the bubbling regime bed.

Table 1. Experimental conditions.

Parameters	Specific Conditions
Static bed height	170 mm
Particle type	Group B Silica sand with mean diameter of 276 microns and density of 2650 kg/m3
ECT sensor	Twin plane, eight measuring electrodes (1 mm long), 200 fps sampling rate
Fluidized bed	59 mm ID, 3 mm wall thickness, 1.5 m long in total
Distributor	Perforated PVC plate, 48 holes of 1 mm diameter with an open area of 1.38%

3 Results and discussion

In order to estimate the bubble rising velocity in the ECT system, a discrete format of the cross-correlation expression is shown in Equation (1) integrated with the signal of the averaged solids volume fraction obtained from the ECT measurement.

$$R_{xy}(\tau)=\frac{1}{N}\sum_{i=1}^{N} x(t)\, y(t+\tau) \tag{1}$$

where x(t) and y(t) are the upper and lower plane signals of the averaged volume fraction, N is the number of samples in the summation, τ is the time lag between the signals of the two measuring planes. Once the time lag of the bubble travelling from the lower plane to the upper plane is derived, the axial bubble rising velocity will be estimated by taking the centre to centre separation distance of 40 mm between two planes into account. The obtained bubbler rising velocity will be compared with two widely used empirical correlations which are presented in Table 2.

Table 2. Empirical correlations for estimating bubble rising velocity.

No.	Authors	Correlations	Particles Group
1	Davidson and Harrison, 1963 [14]	$U_b = U_{br} + (U - U_{mf})$	Group A,B and D
2	Werther, 1978 [15]	$U_b = \varphi\sqrt{gd_b}$ For Geldart B particles: $\varphi = \begin{cases} 0.64 & D \ll 10 \\ 0.254 \times D^{0.4} & 10 < D < 100 \\ 1.6 & D \gg 100 \end{cases}$	Group A,B and D

However, before proceeding, it is necessary to evaluate the system error caused by applying certain sampling rate (in the present case is 200 fps) using the cross-correlation techniques, which many studies have not done so yet. According to previous theory [16], the minimum acquisition time δ can be taken as twice the product of the minimum transit time of the fluid $\Delta\tau$ and the fractional discrimination k. By rearranging this, it gives the following:

$$k = \frac{\delta}{2\Delta\tau} \tag{2}$$

The fractional discrimination is the sensitivity of a velocity measurement system based on its sampling speed. Here, in the present study, the distance between two measuring planes is 0.04 m, the sampling rate is 200 fps and the maximum gas superficial velocity is 8.89 cm/s. By applying Equation (2), subsequently, the fractional discrimination of 0.006 or 0.6% is obtained. Compared with some previous work [17], the system error in the present study is much more acceptable.

The results presented in Fig.3 demonstrate generally that the estimated bubble rising velocity via cross-correlation has the correct trend, i.e. that the bubble rising velocity increases accordingly with the gas superficial velocity compared with the results of Davidson and Werther's empirical correlations. However, the estimated bubble rising velocity has a better agreement with Davidson's equation than Werther's equation. The percentage errors between the cross-correlation results and the results from Davidson's equation are all within 11.7% with the smallest values of 0.8% when the gas superficial velocity was at 8.87 cm/s. However, the largest percentage between the results from cross-correlation and the results from Werther's equation is around 18.4% occurring at a gas superficial velocity of 8.02 cm/s. Furthermore, the estimated values of bubble rising velocity from Werther's equation are mostly lower than the results obtained from both the cross-correlation and Davidson's equation. The reason behind this phenomenon may stem from the original expressions of both equations. The term U_0-U_{mf} which appeared in Davidson's equation is absent from the Werther equation, as indicated in Table 2. Since the U_{mf} is constant, when the superficial velocity increases, the value of the term of U_0-U_{mf} is correspondingly increased.

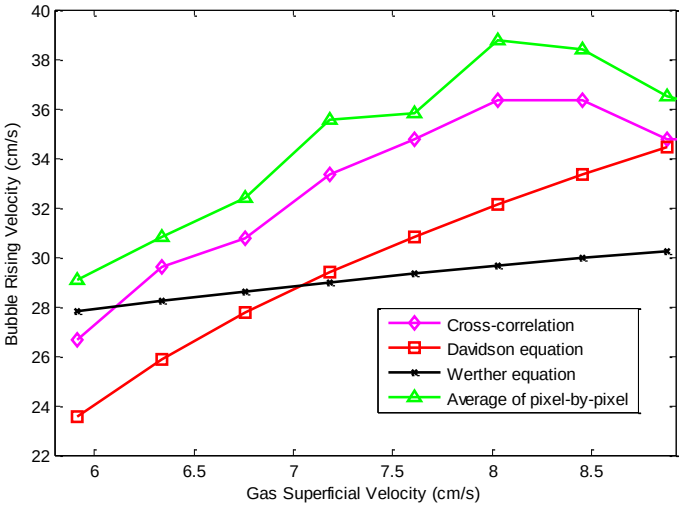

Fig. 3. Comparison of bubble rising velocity between results derived by means of conventional cross-correlation techniques, average of pixel-by-pixel and empirical correlations.

Local three dimensional profiles of the bubble rising velocity can be derived by means of the cross-correlation technique within each pixel of the 812 effective individual pixels of the circular bed pipe cross section. The process is expressed in the following equation:

$$R_{xy}, k(j) = \frac{1}{N} \sum_{i=1}^{N} x_k(i)\, y_k(i + j), \tag{3}$$

where j=0,1,2,…,M; k=1,2,…,812; x(i) and y(i) are the upper and lower plane signals of local solids volume fraction, N is the number of samples in the summation, M is the number of samples in the cross correlation calculation, j is the number of delayed samples, and k is the pixel index. The estimated three dimensional distribution profiles of the bubble rising velocity at two different gas superficial velocities, namely, 5.91 cm/s and 8.45 cm/s are plotted in Fig. 4 and Fig. 5, respectively. X and Y co-ordinates denote the pixel index by row and by column, respectively. The Z co-ordinate represents the value of the axial bubble rising velocity at a specific pixel location.

As it can be seen from Fig. 4, when the gas superficial velocity is low at 5.91 cm/s, the bubble rising velocity can only be extracted on limited pixels. This phenomenon can probably be explained as follows. The fluidization state at lower gas superficial velocities has not been developed or evolved completely. Hence, some areas, especially near wall, have bubbles appearing in a random fashion even with the evenly distributed upward flowing air. In addition, some bubbles may change the moving path in the transverse direction. Subsequently, the bubble rising velocity cannot be detected by means of the cross-correlation technique since the similarity of the two signals is significantly weakened when a bubble is traversing from the lower plane to the upper plane at a specific pixel location.

By observing the three dimensional distribution of the bubble rising velocity in Fig. 5 where the gas superficial velocity was increased to 8.45 cm/s, more and more pixels are able to produce the bubble rising velocity estimated via the cross-correlation. This indicates that the fluidization state is fully developed. Also, there are gradients on the derived bubble rising velocity values. This demonstrates that bubbles appearing over pixels near wall have larger rising velocities compared with the values in the central area pixels. The peak in the Fig. 5 indicates the bubble rising velocity has the maximum value around that corner at that specific gas superficial velocity. The high frequency of bubbles appearing in this region may contribute to these phenomena.

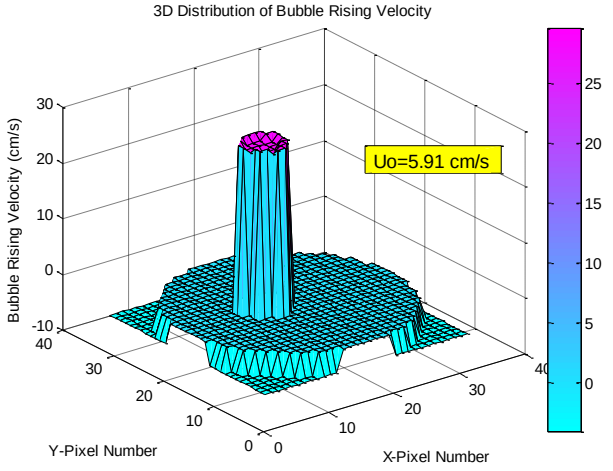

Fig. 4. Three dimensional distribution of bubble rising velocity on a pixel-by-pixel basis derived from the cross-correlation when the gas superficial velocity is at 5.91 cm/s.

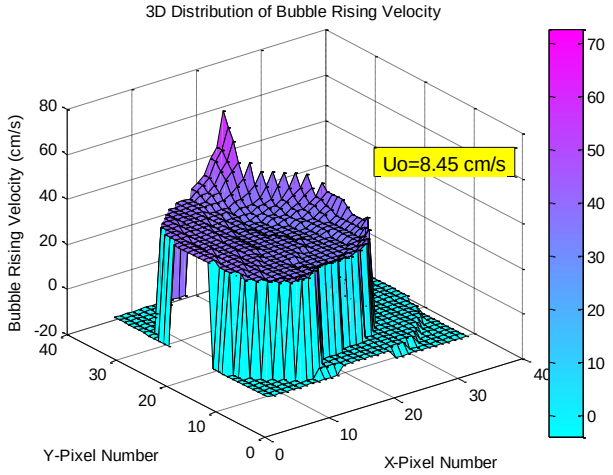

Fig. 5. Three dimensional distribution of bubble rising velocity on a pixel-by-pixel basis derived from the cross-correlation when the gas superficial velocity is at 8.45 cm/s.

In order to evaluate the performance of the three dimensional profile of the bubble rising velocity on a pixel-by-pixel basis, the averaged bubble rising velocity values based on the effective pixels within the 812 pixels are plotted in Fig. 3, compared with the results obtained from the conventional cross-correlation using the averaged volume fraction data and the empirical correlations. The results shown in Fig. 3 display good agreement between the conventional cross-correlation method and the pixel-by-pixel method. Although the results obtained from the averaged value via the pixel-by-pixel method are slightly larger than the cross-correlation results using the averaged volume fraction, the percentage difference between them is in a really low range from 2.9% to 8.4%. It demonstrates again that the cross correlation via local pixel solid fraction is an effective approach in investigating bubble behaviour in a three dimensional manner. It is also interesting to find an increasing trend of the 3D velocity profile across the circular cross section. It may be worth carrying out some estimation to derive bubble diameter from these profile boundaries.

4 Conclusions

A customized twin-plane ECT sensor (with 10 mm measuring electrodes) was designed to investigate the hydrodynamic characteristics inside a bench-scale gas-solids fluidized bed. Conventional cross-correlation techniques were employed to derive the axial bubble rising velocity at various gas superficial velocities. The obtained results demonstrate a good agreement with the results from empirical correlations especially the Davidson equation. Three dimensional axial bubble rising velocity distribution was extracted by means of the cross-correlation techniques on a pixel-by-pixel basis. The velocity profile at 8.45 cm/s shows a more developed effective area than the result for 5.91 cm/s. The bed and bubble behaviour evolution were analysed on a temporal and spatial representation. It is also interesting to find an increase trend of the 3D velocity profile across the circular cross section. Future work can be carried out to estimate bubble diameter from these profile boundaries at various superficial velocities.

The first author would like to acknowledge the maintenance funding from The China Scholarship Council (CSC) and tuition fees funding from the School of Civil Engineering, University of Leeds in support of his PhD programme.

References

1. D. Kunii and O. Levenspiel, Fluidization engineering. Vol. **2**. (1991).
2. S. Sasic, B. Leckner, and F. Johnsson, Prog. Energy Combust. Sci., **33**(5): p. 453-96. (2007).
3. S. Werle and R. K. Wilk, Renew. Energy, **35**(9): p. 1914-9. (2010).
4. Y. T. Makkawi and P. C. Wright, Powder Technol., **148**(2): p. 142-57. (2004).
5. J. Werther, Powder Technol., **102**(1): p. 15-36. (1999).
6. J. t. Werther and O. Molerus, Int. J. Multiphase Flow, **1**(1): p. 103-22. (1973).
7. K. Oki, T. Akehata, and T. Shirai, Powder Technol., **11**(1): p. 51-7. (1975).
8. I. Chan, C. Sishtla, and T. Knowlton, Powder Technol., **53**(3): p. 217-35. (1987).
9. P. Rowe and H. Masson, T I Chem Eng-Lond. **59**(3): p. 177-85. (1981).
10. T. Dyakowski, L. F. Jeanmeure, and A. J. Jaworski, Powder Technol., **112**(3): p. 174-92. (2000).
11. J. Halow, G. Fasching, P. Nicoletti, and J. Spenik, Chem. Eng. Sci., 48(4): p. 643-59. (1993).
12. D. Geldart, Powder Technol., **7**(5): p. 285-92. (1973).
13. X. Li, PhD Thesis, Univ of Leeds. (2016).
14. D. Harrison, R. Clift, and J. F. Davidson, Fluidization. (1985).
15. J. Werther, German Chem Eng., **1**: p. 166-74. (1978).
16. M. Wang, Y. Ma, N. Holliday, Y. Dai, R. A. Williams, and G. Lucas, IEEE Sensors Journal, **5**(2): p. 289-99. (2005).
17. Y. Wu, H. Li, M. Wang, and R. A. Williams, Can. J. Chem. Eng., **83**(1): p. 37-41. (2005).